

Dense high aspect ratio nanostructures for cell chip applications - Fabrication, replication, and cell interactions

Markus Pribyl^a, Philipp Taus^a, Sonia Prado-López^a, Samuele M. Dozio^a, Werner Schrenk^b, Michael J. Haslinger^c, Sonja Kopp^c, Michael Mühlberger^c, Heinz D. Wanzenboeck^{a,*}

^a TU Wien, Institute of Solid State Electronics, Gusshausstraße 25-25a, 1040 Vienna, Austria

^b TU Wien, Center for Micro and Nano Structures, Gusshausstraße 25-25a, 1040 Vienna, Austria

^c PROFACTOR GmbH, Im Stadgut D1, 4407 Steyr, Austria

ARTICLE INFO

Keywords:

Micro-structuring
Nano-structuring
Cell adhesion
Biomedical applications
Surface structuring
Black silicon
Nanoimprint

ABSTRACT

Culturing human cells on the surface of a microchip brings living cells in direct contact with artificial micro-structured surfaces. This work focuses on the effect of high aspect ratio nanostructures – dense nanoneedle arrays – on the mechanical response and proliferation of fibroblasts. We present a fabrication process for micro-patterned chips that feature areas with hierarchical high aspect ratio nanostructures directly adjacent to flat chip areas. The chip was pre-patterned by conventional lithography. We have fabricated “black silicon” arrays of densely packed, sharp, vertical nano-needles for high aspect ratio structures by cryogenic reactive ion etching in an SF₆/O₂ plasma. An essential requirement for many real-life applications is to make such complex high aspect ratio 3D nanostructures available in larger areas. We have successfully demonstrated the 3D replication of black silicon by a UV- nanoimprint lithography process. This study provides insight into the extent to which such nanoneedle arrays influence the growth of human fibroblasts. We have investigated microstructured samples featuring a combination of (i) smooth surfaces and (ii) nanoneedle surfaces for the mechanical behavior and proliferation of fibroblasts. Our results show that the bonding viability and proliferation of the fibroblast on the high aspect ratio nano-needle surfaces differ significantly from flat surfaces. The nanoneedles only provide a minimum area for cell attachment compared to the neighboring flat, unstructured chip areas.

1. Introduction

A widely established research field for in vitro models are organ-on-a-chip technologies [1,2]. In almost every kind of organ-on-a-chip model, cells or cell cultures are in direct contact with, are growing on, or are moving along artificial micro-structured surfaces [3]. Such microstructured and nanostructured surfaces have gained interest as customized surfaces that can either promote or prevent cell growth and cell adhesion [4]. It has been shown that high aspect ratio nano-structured surfaces can change the cell binding and proliferation rate [5,6]. The structure investigated in this study is a high aspect ratio nanostructure array of densely packed, sharp nano-needles, which provides a minimum area for cell attachment. Such structures can be helpful to influence the mechanical response of cells on top of substrates where a plasma process, e.g. to deposit fluoropolymers [7], is not possible because of the type of material. High aspect ratio structures might also be interesting for practical use, like nanopillars that can be

used as electrodes for recording electrical cell potentials or micro and nano capillaries, which have been demonstrated to penetrate the cell membrane and come in contact with the cytoplasm of cells [8]. It is also of interest to develop a process where high aspect ratio structures can be combined with microstructures, e.g., sensor areas where cells are only present at a pre-defined location and are not stochastically scattered on the entire surface of a sensor element. The classical approach to fabricate high aspect ratio nanostructures would be e-beam lithography: By masking a surface with nanodot arrays, it is possible to etch back the substrate, resulting in a variety of single pillars of the substrates [9]. The downside of this e-beam lithography approach is that the sequential exposure of each dot is time-intensive. For large area structuring, the e-beam lithography approach is unsuited. To produce high aspect ratio structures on a larger area several alternative approaches exist including laser ablation [10], metal assisted chemical etching [11], and other specialized etching techniques, such as anodization and etching to receive porous alumina nanostructures [12]. To avoid the bottleneck of

* Corresponding author.

E-mail address: heinz.wanzenboeck@tuwien.ac.at (H.D. Wanzenboeck).

<https://doi.org/10.1016/j.mne.2022.100121>

Received 13 December 2021; Received in revised form 2 February 2022; Accepted 1 March 2022

Available online 3 March 2022

2590-0072/© 2022 The Authors. Published by Elsevier B.V. This is an open access article under the CC BY-NC-ND license (<http://creativecommons.org/licenses/by-nc-nd/4.0/>).

lithographic patterning of each high aspect ratio needle structure, this study focuses on the fabrication of high aspect ratio needle structures by black silicon [13], an anisotropic etch process that uses surface impurities or nanosized residues as a stochastic mask pattern. With its characteristic needle-shaped nano topography, black silicon provides only a minimal surface area for cell growth and can change cell motility, morphology, and viability [14]. Black silicon can cover large surface areas and features needle-shaped structures with a diameter less than 1 μm and a tip radius below 50 nm [15]. The challenge with black silicon is that it is typically created on large surface areas and needs a silicon substrate. For cell-chip applications only confined, preselected chip areas should feature the high aspect ratio nanoneedles, and these structures should also be producible on other substrates than silicon. The transfer of the nanostructures from black silicon onto other substrates can be accomplished by nanoimprint lithography (NIL). Nanoimprint lithography is a well-established process for replicating 3-dimensional structures in one or two steps from a master substrate into or onto different substrates [16,17]. In addition, NIL can also be used as a roll to roll process, where the imprints could be replicated for mass production, which could be helpful to counteract costs [18–20]. To use NIL, we developed a black silicon structuring process to fabricate masters for imprinting. This process can create microstructures that are also nanostructured with a high height/diameter ratio. To illustrate this versatile structure, we manufacture an etched lines and spaces master that features black silicon only on the mesa areas while a flat substrate remains on the bottom of the grooves. We have additionally developed a second inverse process where the black silicon is at the bottom of the grooves, and the mesas are flat. It was tested if black silicon can be replicated and how the structural fidelity of the imprints has changed compared with the master.

A further approach for controlling the biocompatibility and cell mechanical behavior on a surface is surface coating. To enhance the attachment of cells to an artificial surface by protein coatings (e.g., with poly-L-lysine or collagen) is a widely used method. With inorganic surfaces, the coating with self-assembled monolayers is another acknowledged approach. This work also investigates plasma-induced surface modification as a potential route for modifying and controlling the cell material interaction and proliferation on a chip. For organ-on-chip systems, the effect of the surface topography – nanoneedles or flat surface – and the effect of chemical surface termination – hydrophilic or lipophilic – is crucial for the growth, proliferation, and differentiation of cells [21–23]. Depending on the surface structures, even directional cell growth of cells has been reported [24]. In a final phase, we present how samples featuring a combination of smooth surfaces and nanoneedle surfaces would change the morphology of human fibroblasts.

2. Material and methods

2.1. Black silicon fabrication

The substrates for the experiments were fabricated from a single side polished P/B-doped (100) CZ silicon wafer (Siegert Wafer GmbH). The Si substrates were hand-cleaved from the wafer, cleaned in acetone and isopropanol, and dried with N_2 . After cleaning, the substrates were photolithographically patterned using an image-reversal photoresist (AZ 5214 E, Microchemicals GmbH). The photoresist was exposed with a mask aligner (MJB3, wavelength 365 nm, Karl Süss) with a dose of 36 mJ/cm^2 and a chrome-on-glass photomask.

The black silicon (b-Si) areas were fabricated by cryogenic reactive ion etching (RIE) in an SF_6/O_2 plasma (Oxford Plasmalab 100) using etch parameters yielding a highly anisotropic etch progress (see BSP1-BSP3 process for details). For etching we fixed the hand-cleaved Si (100) samples (2–3 cm^2) on top of a 6" Si (100) carrier wafer. Using a Si wafer in contrast to the frequently used quartz carrier ensures a better thermal conductivity between the RIE table and the sample. The drawback of using a Si Wafer is, that the wafer will also be etched in the

RIE which can lead to micro masking and plasma loading. This negative effect was avoided by spin coating the carrier wafer with a 1.6 μm thick AZ 5214 E photoresist, which conveniently also acted as glue between the Si samples and the Si carrier wafer. Baking the carrier sample stack at 120 $^\circ\text{C}$ for 5 min removed volatile products and ensured a solid bonding between sample and carrier.

We developed three distinct etching processes, which are called Black Silicon Process 1 (BSP1), BSP2, and BSP3. An overview of the BSP can be seen in Table 1 and also Supplementary Material Fig. A1 which graphically describes the fabrication process.

For BSP1, the lithographically patterned photoresist acts both as an etch-mask and a source for surface impurities leading to micro masking and the formation of black silicon. While resist-free areas became trenches with a smooth floor, the resist-coated areas became the mesas. With extended etch duration also the photoresist was increasingly etched, and the last remains of the photoresist became a stochastically distributed nano mask for the Si etching, resulting in a black silicon structure on the mesa areas. The cryogenic RIE used a gas mixture and gas flow of 50 sccm SF_6 and 9 sccm O_2 , a set pressure of 1.4 Pa, with 17 W CCP power and 150 W ICP power, a temperature of $-108\text{ }^\circ\text{C}$, and a He backing with a pressure of 1.33 Pa. The etch time was varied to achieve a variation in the height of the black silicon.




With BSP2, the black silicon structures were fabricated in the trenches, while the mesas remained flat Si surfaces. To create black silicon on the surface areas not coated by photoresist, the lithographically patterned substrates were first etched in an Ar plasma with an Ar flow of 10 sccm, a set pressure of 2.67 Pa, 50 W CCP power, at a temperature of 40 $^\circ\text{C}$. After the Ar etching of the trench structures, the substrates have been etched with a second etch step using the previously described cryogenic RIE process BSP1, where the O_2 flow was set at 11 sccm.

The BSP3 creates rough mesas and smooth grooves. The lithographically structured substrates were first etched to the desired depth with the c-RIE process of BSP1 without damaging the photoresist. In the grooves of the substrate, a Cr hard mask was sputter-deposited, and the substrate was patterned in a liftoff step. The Cr hard mask hinders the development of black silicon in the grooves. Then, the substrate was etched with the etch process of BSP2. Finally, the Cr in the grooves have been removed in a Cr-Etch (Chrome Etch 18, micro resist technology GmbH).

2.2. Formation and control of hydrophobic surfaces

Hydrophobic areas have been fabricated with an RIE (Oxford Plasmapro 100) process. For patterned surface modification, a photolithographic pattern from 5214 E photoresist was manufactured on the chip surface. On the patterned and non-patterned surfaces of the substrates, a fluoropolymer layer was deposited from trifluoromethane (CHF_3). Process parameters were 50 W RF Power, 85 sccm CHF_3 , a pressure of 11.33 Pa, and the total duration was 10 min. After deposition of the fluorine-terminated surface layer, the photoresist mask of the patterned

Table 1
Black Silicon Process overview.

| Process | Pattern | Mask material | Black Si on | Illustration |
|---------|---------------------------------------|------------------------|-----------------|---------------------------------------------------------------------------------------|
| BSP1 | Lines & Spaces 56 / 200 μm | Photoresist | top (mesa) |  |
| BSP2 | Lines & Spaces 76 / 200 μm | Photoresist | bottom (groove) |  |
| BSP3 | Lines & Spaces 76 / 200 μm | Photoresist & Chromium | top (mesa) |  |

substrates has been removed, and the samples have been cleaned with acetone. The hydrophobicity has been tested and quantified by measuring the contact angle between the substrate and deionized (DI) water. A water droplet of 10 μL has been placed on top of the surfaces and has been photographed (see also Supplementary Material Fig. A2). This procedure was repeated four times per substrate, and we measured the contact angle with ImageJ [25].

2.3. Imprinting

The high aspect ratio nanoneedles of black silicon were replicated by UV-nanoimprint lithography (NIL) in a 2-step replication process, which is sketched in Supplementary Material Fig. A3. From the original master in the first step, a working stamp with the complementary structure was fabricated (Fig. A3 a–c). In the second step (Fig. A3 d – e), we used this working stamp to fabricate an imprint replica featuring the nanoneedle arrays of black silicon. For the imprint material, i.e., the material that forms the imprinted nanoneedles, we used OrmoComp® (OC) (micro resist Technology GmbH). First, the black silicon master was treated with BGL-GZ-83 as an anti-adhesion layer [26]. Working stamps were prepared using Fluorolink® MD 700 (Solvay) with Irgacure® 1173 (BASF) as the photoinitiator. A 300 μm thick PVC foil was activated in an oxygen plasma (Diener electronic GmbH + Co. KG) and was used as a backplane for the stamps. The stamp material was dropped on the master, then the PVC foil was brought into contact, and UV-curing was carried out at 365 nm (UV-LED, 9500 mJ/cm^2) (Fig. A3 a and b). The PVC foil with the nanostructured MD700 could then be removed from the master (Fig. A3 c) and be further used as a working stamp. The substrates used for imprinting were standard microscope slides (25.4 \times 25.4 mm^2 , 1 mm thickness, Paul Marienfeld GmbH), cleaned with water, acetone and activated in an oxygen plasma. OrmoComp® was dispensed dropwise onto the stamp and the substrate (Fig. A3 d). We took care to avoid any air bubbles when contacting the stamp and substrate, which was done in a smooth rolling motion from one end of the stamp to the other. Another important aspect to achieve bubble-free imprints is to make sure that no bubbles are present in the resin after dispensing. UV-curing at 365 nm (UV-LED, 9500 mJ/cm^2) and careful manual separation of imprint and stamp concluded the nanoimprinting procedure (Fig. A3 e and f).

2.4. Biological material and culture conditions

The Human Dermal Fibroblasts cell line HDF (Sigma) was employed to evaluate black silicon's effects and the fluoropolymer coating on cellular viability. For that, we deposited the cited materials on 12 well tissue culture plates (CELLSTAR). Next, we seeded 30.000 cells per well. Also, we seeded cells on plastic (polystyrene) as a control. The cells were cultured for 2, 3, and 7 days under an atmosphere containing 5% CO_2 at 37 °C in a media consisting of Dulbecco's Modified Eagle's Medium (Lonza, USA) supplemented with 10% bovine calf serum (Sigma-Aldrich) and penicillin/streptomycin (Lonza, USA), at a working concentration of 100 units of potassium penicillin and 100 g of streptomycin sulfate per 1 mL of culture media (Sigma-Aldrich).

2.4.1. Cell viability and cell density

To evaluate the cell viability, we stained the cells with Hoechst 33342 and Propidium Iodide (PI) (Sigma-Aldrich) after 2, 3, and 7 days in culture on the top of materials. Propidium iodide can only enter dead or dying cells with compromised plasmatic membranes and emits red fluorescence when bound to DNA. Hoechst 33342 stains the DNA of both living and dead cells. We used Hoechst to label the total number of cells and PI to estimate the number of cells dead on the cells growing on the different materials and plastic (control). Cell staining was visualized using the inverted microscope NIKON ECLIPSE TE200 and images were recorded with a Hamamatsu camera system. Positive control for cell death was done in one cell culture. For this, we added 0.4 mM hydrogen

peroxide H_2O_2 to our cultures and incubated them for 24 h. Finally, we calculated the cell density per area using the ImageJ software. We built the graphs with OriginPro (OriginLab) and did a one-way Analysis of variance (ANOVA) with the same software. Also, we analyzed the cells' nuclear morphology to precisely estimate the number of cells undergoing cell death that may escape PI staining. For this, we used the protocol described by [27]. Three image sections of the Hoechst staining per material were evaluated.

2.4.2. Cell morphology and distribution

We analyzed the cell morphology, distribution, and orientation on top of the different materials. For this, we fixed the cells with paraformaldehyde 4% (Sigma-Aldrich) and permeabilized them with Triton 0.5% (Merck). Next, we stained the cytoskeleton of the cells with Phalloidin-488 (Abcam) that links to F-Actin. We also stained the cell nuclei with DAPI (Sigma). We used the inverted microscope NIKON ECLIPSE TE200 to visualize the cell morphology and orientation on the different materials and plastic.

2.4.3. Scanning electron microscopy (SEM)

To better understand the morphological changes of HDF on the different materials, the seeded samples were fixed for SEM observation after 48 h of culture. The samples were washed with PBS solution and fixed using a 3% Glutaraldehyde solution for 1 h at 4 °C. After removing the fixative solution, the samples were dehydrated via incremental ethanol gradient, followed by hexamethyldisilazane (HMDS) chemical drying. Subsequently, the samples were sputter-coated with a layer of 20 nm Au and examined in a scanning electron microscope (SEM) (FIB Zeiss NEON 40EsB CrossBeam).

3. Results / discussion

To investigate the cell viability on high aspect ratio structures, we have fabricated silicon substrates that feature flat, smooth surfaces adjacent to spiky surfaces with nanoneedle arrays. By combining photolithography for patterning with anisotropic etching to fabricate black silicon surfaces, we could generate high aspect ratio structures in the trenches (grooves) and on the mesas. In the first section, we report on the fabrication and replication of the nanostructures. In the second part, we discuss the biological implication of nanostructures.

3.1. Black silicon fabrication

The etch processes are described in Section 2.1, where we developed different methods to fabricate black silicon. By variations (i) of the process sequence of lithography and etching (BSP1), (ii) by using purely anisotropic etching or mixed anisotropic-isotropic etching processes (BSP2), and (iii), by using either a photoresist mask or a chrome hard mask during etching (BSP3), a wide variety of different structures can be fabricated. Fig. 1 shows designs that can be fabricated with the b-Si etching approach. Fig. 1 a) depicts a substrate structured only with black silicon with a height of approx. 3.6 μm , fabricated with BSP1. This substrate can be used for further structuring. In a subsequent step, it is possible to locally etch away the nanostructures again to yield areas with a flat, smooth surface. Fig. 1 b) shows a substrate with smooth grooves and nanostructured mesas fabricated with BSP2. The height of the mesa is approx. 5.9 μm . Fig. 1 c) depicts the inverted case of Fig. 1 b), where the grooves are nanostructured, and the mesas are smooth, fabricated with BSP3, with a height of approx. 4.7 μm . Fig. 1 d) illustrates a substrate with the maximal achieved depth of process BSP 1. For the b-Si substrates the BSP1 etching process (as shown in Fig. 1 d) resulted in high aspect ratio structures. A median height-to-width aspect ratio greater than 31:1 was extracted from a close-up image of the sample displayed in Supplementary Fig. A4. This value was extracted for a set of 12 pillars. The grooves of the mesoscopic line and spaces pattern are approx. 58 μm in height with smooth walls. The lines are nanostructured

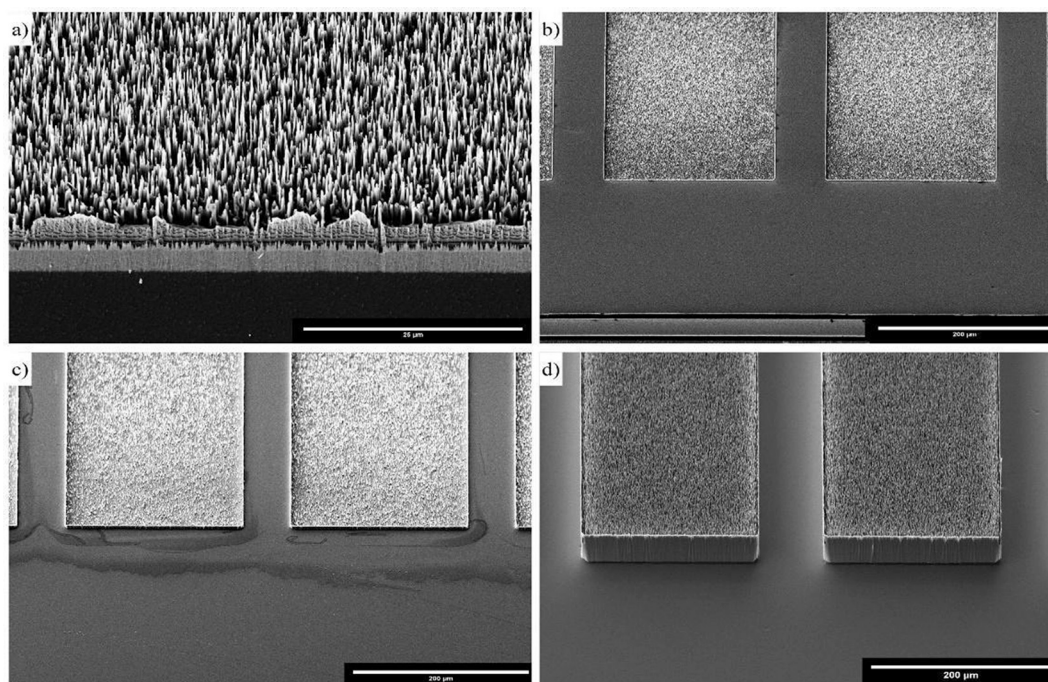


Fig. 1. Overview images of the black silicon after cryogenic RIE etching. Scanning electron microscopy images (45° tilted) show a) the close-up of a cross-section through the cleavage site of an unstructured b-Si surface on a Si-wafer, and (b-d) the front section of rectangular lines of lithographically prepatterned b-Si areas. In total, more than 30 samples were investigated. Selected examples include (b) trench areas with b-Si separated by unstructured, flat mesas (c) mesa areas with b-Si separated by flat groove/trench, (d) mesa with b-Si separated by flat grooves. Scale bars: a) 20 μm , b-d) 200 μm . The structure height and aspect ratio was extracted from high magnification images added as supplementary figure (Fig. A4).

with a b-Si surface. For this b-Si surface the total height of the pillars was measured from the tip to the deepest trench and compared to the full width of the pillar at half height. On selected positions at the rim of the b-Si areas even pillars with an height-to-width aspect ratio exceeding 100:1 were observed, which demonstrates the basic feasibility of fabrication of such high-aspect-ratio structures. However, for cell chip applications (Section 3.3) not the total aspect ratio of the pillar, but rather the geometry of the conical tip section is relevant. Later on, for assessing the cell-tip interaction not the height-to-width aspect ratio but rather the opening angle of the tip cone was measured and used to interpret the biocompatibility and the interaction with living cells.

3.2. Formation and control of hydrophobic surfaces

We structured our samples with a hydrophobic surface coating using a plasma process with CHF_3 , as described in Section 2.2. To assess the hydrophobicity of our samples, the CHF_3 treated surface was investigated by contact angle measurement with deionized water. The contact angle of the CHF_3 -treated areas was 99.5 ± 4.9 degrees, in contrast to the Si substrate, which had a contact angle of 33.5 ± 4.7 degrees. This indicates already a good hydrophobicity of the surface: with 99.5 degrees contact angle, this is already close to the 109 degrees contact angle of water on octadecyltrichlorosilane monolayers [28] on Si, which is a widely used coating to generate hydrophobic surfaces.

3.3. Replication by NIL

For various biomedical applications, such high aspect ratio structures are required on materials other than (optical opaque) silicon or on larger areas. The microfabrication of Si-substrates in Fig. 1 is a multi-step process sequence, and simple one-step fabrication procedures are desirable. Addressing these shortcomings of the Si-based fabrication process, we have developed a method to replicate the patterned high-aspect-ratio structures using an imprint process. With our etching

protocol, black silicon masters have been fabricated to test if we can copy them utilizing NIL as described in Section 2.3. We opted to fabricate specimen without any microstructures for this step because we were only interested in replicating the high aspect ratio nanostructures. We took effort to avoid any micro- or mesoscopic air bubbles when contacting the stamp and substrate by following means: It was optically checked after dispensing that no visible bubbles are present in the resin, and the imprint process was performed in a smooth rolling motion from one end of the stamp to the other. Images of the imprints showed no complete deletions of micropillars or other indications of meso- and microbubbles. Also the cavity-free sidewalls of the imprinted micropillars show now indication of nanobubbles. The peculiar shape of the tip of the micropillars in Fig. 2 is similar among the Si master (Fig. 2a) and its NIL-replicate (Fig. 2b). The flexible working stamp holding the complementary structure, a nanohole array, is not illustrated, since it does not add any additional information on the replication quality. As the b-Si surfaced were fabricated for cell chip applications not the height-to-width aspect ratio of the micropillar but rather the geometry of the conical tip section was measured. The cell layer is interacting with the tip section and the influence of different nanocone geometry on the complex cellular behavior such as cell adhesion has already been described in [29].

For this purpose the opening angle of the tip cone was measured and used to interpret the biocompatibility and the interaction with living cells. Fig. 2 a) shows the master with black silicon needles and a tip half angle of $7.7^\circ \pm 1.1^\circ$. The SEM image of the original master was recorded before imprinting. A cross-sectional image of this sample is also shown in the supplemental Fig. A5a and shows a mean height of $11.1 \pm 1.0 \mu\text{m}$. This b-Si structure was replicated in a 2-step imprinting process to yield an replica structure in NIL resin. Fig. 2 b) depicts the OrmoComp imprints of the master (as depicted in Fig. 2a). A cross-sectional image of this imprinted replica also shown in the supplemental Fig. A5b and shows a mean height of $11.7 \pm 1.2 \mu\text{m}$. The tip half angle was $8.6^\circ \pm 1.2^\circ$. Evaluation has been performed on 12 tips of the master and the

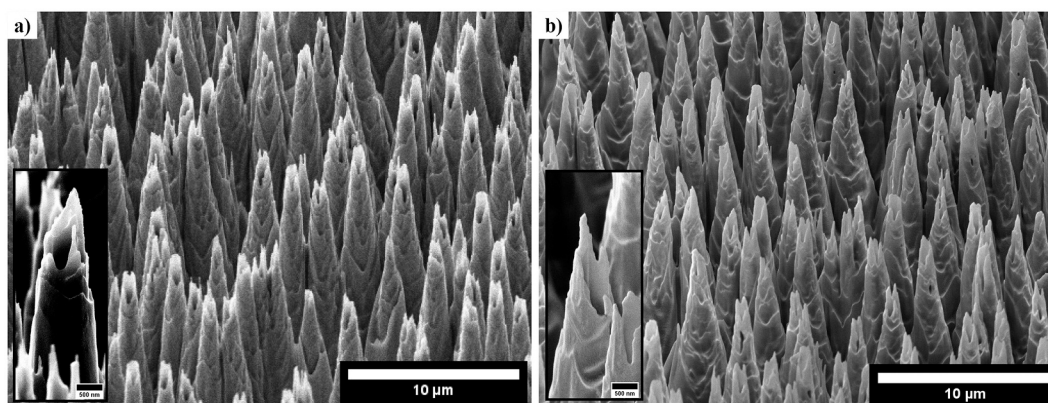


Fig. 2. Replication of black silicon: a) Black silicon master, inset: tip detail of black silicon master b) Black silicon imprint in OrmoComp, inset: tip detail of black silicon imprint. Scale bars 10 µm, Scale bars insets 500 nm.

identical imprint in order to avoid effects by the variation among different imprints (see also Supplementary Material Fig. A5 for higher magnification images). This result indicates a good structure fidelity between master and replica. This demonstrates the technical feasibility to replicate such surfaces also on larger areas using NIL methods, which may become relevant for future cell chip sensors. Surfaces with such dense nanopillar arrays with conical tip sections have been investigated as growth substrates for living human fibroblasts as described in Section 3.5.

With this replication step, the nano structures have been successfully transferred to a new substrate, a glass substrate, as it is frequently used for lab-on-chip systems. While the fabrication of the original stamp structures in the cleanroom required several hours, replicating with the flexible working stamp took minutes. The process is highly repeatable as far as we could investigate so far, however the adhesion between stamp material and backplane of the working stamp still can be improved to achieve a longer stamp lifetime and reduced process costs. Optimizing the backplane treatment in the working stamp fabrication process will be part of future work.

3.4. Cell material interactions

For biomedical applications, it is critical to control the interactions between cells and different surfaces. For applications like drug screening, using nanoelectrode arrays as sensor elements, it is crucial to control the cell growth and orientation on specific sensor areas. We investigate the effect of different structured and coated nano surfaces (S1, S2, S3, S4, and S5) on cell viability, density, and distribution of HDF, see Table 2; also see Supplementary Material Fig. A6.

3.5. Cell viability cell density

We observe between 1 and 3% of cells with double staining for Hoechst and PI in our cultures. It is known that PI does not stain live cells and early apoptotic cells, since their plasma membrane is still intact [30]. An example of the viability results is Fig. 3 that shows HDF cells growing on material S1 after 2 days in culture and a positive death control on the same material after incubation with 0.4 mM H₂O₂ for 24 h. The rest of the images for the Hoechst 33342 and PI staining of HDF growing on (S2, S3, S4, S5, and plastic (polystyrene)) are shown in

Supplementary Material Fig. A7. Also, the Supplementary Material Fig. A8 show the number of normal nuclei in our cultures after nuclear morphology inspection. The plastic presents the higher proportion of healthy cells with normal nuclei, 96% at 48 h, 98% at 72 h, and 99% at 7 days. The amount of normal nuclei observed for the other materials were at 48 h (S1: 88%, S2: 86%, S3: 82%, S4: 81% and S5: 79%); at 72 h (S1: 81%, S2: 91%, S3: 85%, S4: 88% and S5: 84%) and at 7 days (S1: 86%, S2: 88%, S3: 92%, S4: 88% and S5: 91%).

Our results indicate that the studied materials are noncytotoxic. Levels up to 20% of cell death were reported in fibroblast healthy cultures [31]. To further evaluate the influence of the different materials on cell proliferation, we performed a systematic cell count of the fibroblast-stained nucleus at days 2, 3, and 7 after seeding. We counted the cells on a section of the surface that had an area of 3300 × 3300 µm² after Hoechst 33342 and PI staining. The obtained number of cells Hoechst/PI- is shown on Supplementary Material Table A1. According to our results, the material that presents the highest cell density at day 7 is the plastic, followed by the materials S1, S3, S5, and S2 being S4, which gives the smallest cell density at this time point. The cell amounts present in S1 compared to plastic was 2.6-fold lower, in S3 and S5 was 3.6-fold lower, in S2 3.9-fold and on S4 8.7-fold lower. Our results suggest an influence of the Black Silicon structured surfaces and the CHF₃ anti-adherence treatment pattern on cell proliferation between the different materials. The material S1, with the needle-like design, presents the highest cell proliferation rate compared to the plastic. Material S4, where all the surface was fully coated with the CHF₃ fluoropolymer, shows the lowest proliferation compared to the control. The other materials offer different degrees of proliferation according to the pattern distribution of treated and untreated surfaces. Several works have shown the cellular antibonding properties of fluoropolymer coatings in various types of cells [32]. These properties are due to the generation of low surface tension induced by hydrophobic treatment [33]. As for the silicon needles, several studies show distinct effects of nanotopography on fibroblast cell proliferation and binding; in some cases, it is shown that they induce and in others that they prevent them [14]. Interestingly Choi et al. [34] showed that the growth of the fibroblast onto three-dimensional silicon structures is strongly influenced by the size of the needles and the distance between them. We concluded that the different architectures might directly influence the formation of the binding molecules complex in the fibroblast. To further investigate the effect of

Table 2

Specimen overview for cell material interaction experiments.

| S1 | S2 | S3 | S4 | S5 |
|---------------------------------------------------------|----------------------------------------------------------|---------------------------------------------------------|------------------------------------|----------------------|
| 200 µm lines black silicon, 56 µm lines plain substrate | 56 µm lines, fluoropolymer, 200 µm lines plain substrate | 200 µm lines fluoropolymer, 56 µm lines plain substrate | Silicon covered with fluoropolymer | Unstructured silicon |

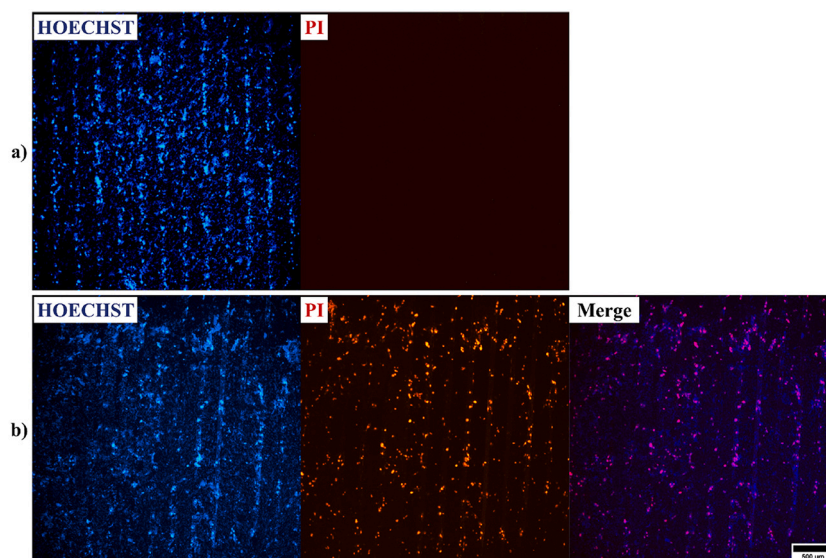


Fig. 3. a) Cell viability assay of HDF-cells, 4× magnification on S1 after 2 days on culture, b) Dead positive control of HDF after growing 2 days on S1. Death was induced with hydrogen peroxide H₂O₂. Hoechst staining in blue, PI staining in red, and Merge. Scale bar: 500 µm. (For interpretation of the references to colour in this figure legend, the reader is referred to the web version of this article.)

the Black Silicon structured Si surfaces, non-structured surfaces, and the CHF₃ hydrophobic treatment on the HDF cell behavior. Next, we looked at the cell distribution and disposition of the HDF cells in our cultures.

3.6. Cell distribution and orientation

Our results show a distinct distribution of the cells among the treated and untreated areas of the materials and between the different materials, see Fig. 4 and Fig. 5. The cells grow preferentially on the untreated areas of all the materials (areas without needles and surfaces without fluoropolymer).

The number of cells detected in the treated areas (coated with fluoropolymer or structured with silicon needles) was significantly smaller, especially at days 2 and 3. The most significant difference between the treated and untreated areas was observed on day 2 on the material S2, and it persisted on time. The number of cells on the treated areas

increased on day seven: S1 (33% treated 67% untreated), S2 (5,8% treated 94,7% untreated), and S3 (15% treated 85% untreated). The presence of some cells in the treated areas at day 7 can be explained by the capacity of some of the cells to use their filopodia to anchor themselves to the texturized areas with needles [35]. Also, the fibroblast's secretion of extracellular matrix growing in the close untreated areas can favor the cell material cohesiveness [36]. The same effect was observed on S4 that presents HDF cells growing at day 7 despite the CHF₃ treatment. Nevertheless, on days 2 and 3, the number of cells on this material was poor, and the distribution was random and patchy (images not shown).

Interestingly, we observed that the materials (S1, S2, and S3) induce cell orientation (see Fig. 5). Several works show how nano-topographical alignment can cause cell alignment and orientation. It was suggested that this orientation effect results from mechanical cues that resulted in cell spreading and elongation by contact guide effects

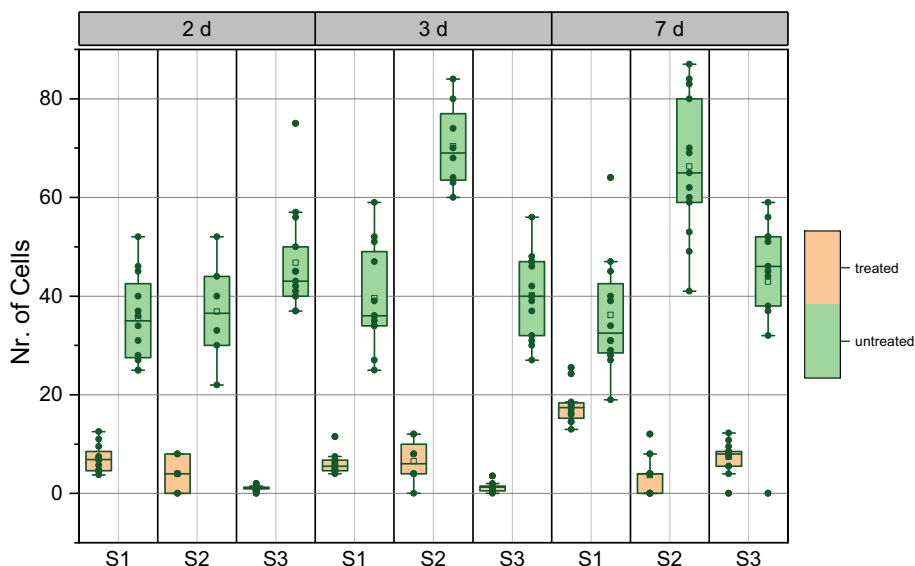


Fig. 4. Number of cells on top of substrates for three-time points. Nr. of cells normed to the equal area. S1: Black Silicon, S2: CHF₃ structured lines 56 µm width, S3: CHF₃ structured lines 200 µm width.

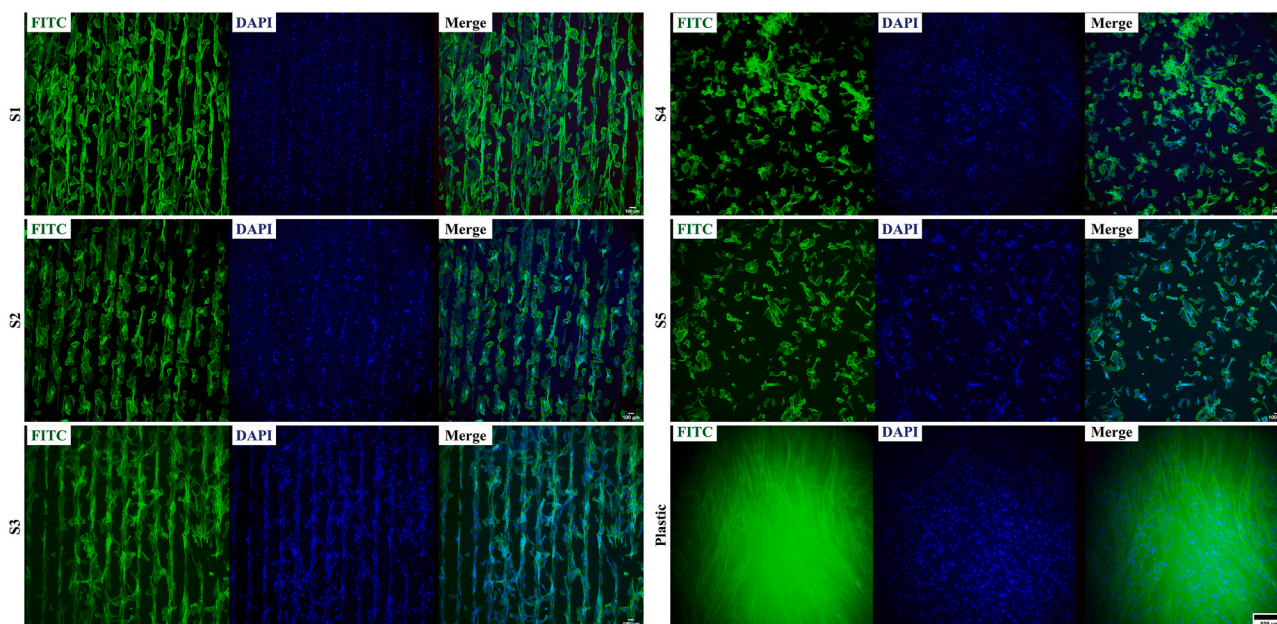


Fig. 5. HDF human fibroblast growth on S1: Black Silicon, S2: CHF₃ treated lines 56 μm width, S3: CHF₃ treated lines 200 μm width, S4: CHF₃ treated Si, S5: uncoated Si, and Plastic. 4× magnification. Phalloidin staining (F-Actin) in FITC, Nucleus staining in DAPI. Scale bar lower right 500 μm.

[37]. In contrast, materials S4 and S5 that are flat presented a random distribution of fibroblast and lack of cellular directionality. Our results show that combining both coated and uncoated areas or structured and unstructured areas of black silicon induces cell orientation. To have control in vitro the spatial distribution and direction of cells is a valuable feature in bioengineering applications since it will help us mimic the natural tissue.

3.7. Cell distribution and orientation scanning electron microscopy (SEM)

To study in further detail the cell distribution and orientation on the different materials, we used scanning electron microscopy (SEM), see Fig. 6. In (S1), we observed that the fibroblast on the nanoneedles structured surfaces are less elongated and more rounded than those that grow on flat surfaces, which indicates a weak bond to the substrate [23]. Furthermore, they did not present orientation being randomly distributed over the surface of the substrate. Conversely, the fibroblast growing on the flat surfaces were more elongated and grew in a predetermined way. These results put in evidence that the non-nanostructured areas are preferred by the cells. The images for the remaining materials are in Supplementary Materials Fig. A9. Our results show that the cells are

situated preferentially in the uncoated areas of the materials and display an elongated form (S2, S3). Also, they start to present specific cell arrangements (S2, S3). This arrangement will become more evident at day 7 in culture, as shown previously in Fig. 6. In the plastic control and the uncoated material, the cells grew to present no preferred orientation.

4. Conclusions

We presented a fabrication process for micro and nanostructuring of substrates. We have fabricated hierarchical high aspect ratio structures, which exceed structures fabricated with e-beam lithography and are confined to well-defined areas. We have shown that established in-silicon technology is only needed to manufacture a first silicon master. Further high aspect ratio structures can be replicated with NIL, a low cost-efficient single-step process. With NIL many different production methods would open up, with a structured master, it would be possible to create a flexible working stamp, which would allow the imprinting of 3D structures on non-even curved surfaces, which would not be possible using standard microfabrication methods. Furthermore, this process is a promising production method for fast replication of the nanostructures. By NIL such nanostructures can be replicated on a substrate or on

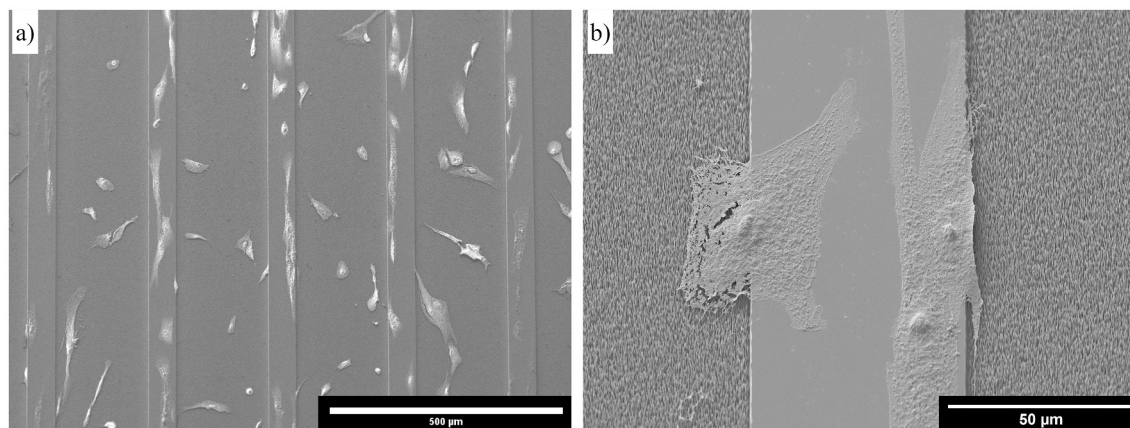


Fig. 6. SEM image of cells seeded on Sample S1 a) Overview sample S1 Scale bar: 500 μm, b) Magnified region of S1 Scale bar: 50 μm.

selected areas that have been previously defined by lithography. The generated structures can be used to control the mechanical cell behavior. Both, topographic patterning by Si nanoneedles as well as chemical patterning by CHF₃ polymeric treatment were efficacious in regulating cell growth. Furthermore, we showed that the combination of structured and unstructured areas or the coated and uncoated regions in the same material can induce cell alignment and orientation. This has a significant impact on engineering applications, where mimicking the natural tissue structure is critical. Indeed, this has potential future applications for reference areas for sensors. Nanoneedle patterning and CHF₃ treatment would be a preferable approach to avoid cell growth on specific areas or for other applications where cell binding and proliferation should be countered, for example, microfluidic channels.

Funding

The present work was supported by the Austrian Research Promotion Agency (FFG) under the call “Production of the Future” with grant number 871438 (project NEAT).

Declaration of Competing Interest

The authors declare that they have no known competing financial interests or personal relationships that could have appeared to influence the work reported in this paper.

Acknowledgments

The concept to design of cell arrays consisting of high and low attachment areas with the indicated dimensions was contributed by ChanPharm GmbH (Austria) (see WO 2021/083885; PCT/EP 202/080163). Additionally, we would like to acknowledge the expertise of our project partners the Institute of Molecular Biotechnology Austria and Stensborg A/S (Denmark) for their advisory activity.

Appendix A. Supplementary data

Supplementary data to this article can be found online at <https://doi.org/10.1016/j.mne.2022.100121>.

References

- [1] “Kratz et al 2019_Latest Trends in Biosensing for Microphysiological Organs-on-a-Chip and.pdf.” Accessed: Jul. 30, 2021. [Online]. Available: <https://www.mdpi.com/2079-6374/9/3/110/pdf>.
- [2] “Bhatia und Ingber - 2014 - Microfluidic organs-on-chips.pdf.” Accessed: Jul. 30, 2021. [Online]. Available: <https://www.nature.com/articles/nbt.2989.pdf>.
- [3] “Kitsara und Ducr e - 2013 - Integration of functional materials and surface mo.pdf.” Accessed: Oct. 19, 2021. [Online]. Available: <https://iopscience.iop.org/article/10.1088/0960-1317/23/3/033001/pdf>.
- [4] “Zhang et al. - 2008 - Attachment and detachment of living cells on modif.pdf.”
- [5] “Higgins et al 2020_High-Aspect-Ratio Nanostructured Surfaces as Biological Metamaterials.pdf.” Accessed: Jul. 30, 2021. [Online]. Available: <https://spiral.imperial.ac.uk/bitstream/10044/1/74484/2/2019-Higgins-AdvMater-accepted.pdf>.
- [6] T.-J. Ko, et al., Adhesion behavior of mouse liver cancer cells on nanostructured superhydrophobic and superhydrophilic surfaces, *Soft Matter* 9 (36) (2013) 8705, doi: 10/gmcm6b.
- [7] “J rvinen et al 2020_Simultaneous Culturing of Cell Monolayers and Spheroids on a Single.pdf.” Accessed: Nov. 17, 2021. [Online]. Available: <https://onlinelibrary.wiley.com/doi/pdfdirect/10.1002/adfm.202000479>.
- [8] G. He, N. Hu, A.M. Xu, X. Li, Y. Zhao, X. Xie, Nanoneedle platforms: the many ways to pierce the cell membrane, *Adv. Funct. Mater.* 30 (21) (May 2020) 1909890, doi: 10/gm5x5v.
- [9] Y.Q. Fu, et al., Deep reactive ion etching as a tool for nanostructure fabrication, *J. Vac. Sci. Technol. B Microelectron. Nanometer Struct.* 27 (3) (2009) 1520, doi: 10/fkbtnt.
- [10] A.V. Kabashin, et al., Nanofabrication with pulsed lasers, *Nanoscale Res. Lett.* 5 (3) (Mar. 2010) 454–463, doi: 10/ds7gzz.
- [11] C. Huo, et al., Metal-assisted chemical etching of silicon in oxidizing HF solutions: origin, mechanism, development, and black silicon solar cell application, *Adv. Funct. Mater.* 30 (52) (Dec. 2020) 2005744, doi: 10/gn4z49.
- [12] T. Yanagishita, T. Kondo, K. Nishio, H. Masuda, Optimization of antireflection structures of polymer based on nanoimprinting using anodic porous alumina, *J. Vac. Sci. Technol. B Microelectron. Nanometer Struct.* 26 (6) (Nov. 2008) 1856–1859, doi: 10/cdfxfx.
- [13] X. Liu, P.R. Coxon, M. Peters, B. Hoex, J.M. Cole, D.J. Fray, Black silicon: fabrication methods, properties and solar energy applications, *Energy Environ. Sci.* 7 (10) (2014) 3223–3263, doi: 10/gm5zr2.
- [14] J.M. Lopacińska, et al., Cell motility, morphology, viability and proliferation in response to nanotopography on silicon black, *Nanoscale* 4 (12) (2012) 3739, doi: 10/gm5zfd.
- [15] M. Gaudig, et al., Properties of black silicon obtained at room-temperature by different plasma modes, *J. Vac. Sci. Technol. Vac. Surf. Films* 33 (5) (Sep. 2015) 05E132, doi: 10/gm5zcr.
- [16] L.J. Guo, Nanoimprint lithography: methods and material requirements, *Adv. Mater.* 19 (4) (Feb. 2007) 495–513, doi: 10/bgcdqf.
- [17] H. Schiff, Nanoimprint lithography: An old story in modern times? A review, *J. Vac. Sci. Technol. B Microelectron. Nanometer Struct.* 26 (2) (2008) 458, doi: 10/fnsgkx.
- [18] J.-S. Wi, et al., Facile three-dimensional nanoarchitecturing of double-bent gold strips on roll-to-roll nanoimprinted transparent nanogratings for flexible and scalable plasmonic sensors, *Nanoscale* 9 (4) (2017) 1398–1402, doi: 10/gmbknd.
- [19] N. Kooy, K. Mohamed, L.T. Pin, O.S. Guan, A review of roll-to-roll nanoimprint lithography, *Nanoscale Res. Lett.* 9 (1) (Dec. 2014) 320, doi: 10/gj7bbs.
- [20] S.H. Ahn, L.J. Guo, Large-area roll-to-roll and roll-to-plate nanoimprint lithography: a step toward high-throughput application of continuous nanoimprinting, *ACS Nano* 3 (8) (Aug. 2009) 2304–2310, doi: 10/c33f2v.
- [21] E.T. Den Braber, J.E. de Ruijter, H.T.J. Smits, L.A. Ginsel, A.F. von Recum, J. A. Jansen, Effect of parallel surface microgrooves and surface energy on cell growth, *J. Biomed. Mater. Res.* 29 (4) (Apr. 1995) 511–518, doi: 10/cr8v2j.
- [22] R. Gristina, et al., Increasing cell adhesion on plasma deposited fluorocarbon coatings by changing the surface topography, *J Biomed Mater Res B Appl Biomater* 88B (1) (Jan. 2009) 139–149, doi: 10/bqpk73.
- [23] K. Anselme, L. Ploux, A. Ponche, Cell/material interfaces: influence of surface chemistry and surface topography on cell adhesion, *J. Adhes. Sci. Technol.* 24 (5) (Jan. 2010) 831–852, doi: 10/d2ttmq.
- [24] C. Simitzi, A. Ranella, E. Stratakis, Controlling the morphology and outgrowth of nerve and neuroglial cells: the effect of surface topography, *Acta Biomater.* 51 (Mar. 2017) 21–52, doi: 10/f9k28m.
- [25] C.A. Schneider, W.S. Rasband, K.W. Eliceiri, NIH image to ImageJ: 25 years of image analysis, *Nat. Methods* 9 (7) (Jul. 2012) 671–675, doi: 10/gcwb4q.
- [26] M. M hlberger, et al., UV-NIL with working stamps made from Ormstamp, *Microelectron. Eng.* 86 (4–6) (Apr. 2009) 691–693, doi: 10/b32vrs.
- [27] B.S. Cummings, R.G. Schnellmann, Measurement of cell death in mammalian cells, *Curr. Protoc.* 1 (8) (Aug. 2021) doi: 10/gpbxpx.
- [28] M.-H. Jung, H.-S. Choi, Characterization of octadecyltrichlorosilane self-assembled monolayers on silicon (100) surface, *Korean J. Chem. Eng.* 26 (6) (Nov. 2009) 1778–1784, doi: 10/bvwmts.
- [29] L. Purwaningsih, T. Schoen, T. Wolfram, C. Pacholski, J.P. Spatz, Fabrication of multi-parametric platforms based on nanocone arrays for determination of cellular response, *Beilstein J. Nanotechnol.* 2 (Sep. 2011) 545–551, doi: 10/cjkjmn.
- [30] A.M. Rieger, K.L. Nelson, J.D. Konowalchuk, D.R. Barreda, Modified annexin V/propidium iodide apoptosis assay for accurate assessment of cell death, *J. Vis. Exp.* (Apr. 2011) 2597, no. 50. doi: 10/cwvwng.
- [31] A.-S. Gary, P.J. Rochette, Apoptosis, the only cell death pathway that can be measured in human diploid dermal fibroblasts following lethal UVB irradiation, *Sci. Rep.* 10 (1) (Dec. 2020) 18946, doi: 10/gpbxzd.
- [32] F.F.R. Damanik, T.C. Rothuizen, C. van Blitterswijk, J.I. Rotmans, L. Moroni, Towards an in vitro model mimicking the foreign body response: tailoring the surface properties of biomaterials to modulate extracellular matrix, *Sci. Rep.* 4 (1) (May 2015) 6325, doi: 10/gmnmn5.
- [33] S. Parvate, P. Dixit, S. Chattopadhyay, Superhydrophobic surfaces: insights from theory and experiment, *J. Phys. Chem. B* 124 (8) (Feb. 2020) 1323–1360, doi: 10/gg48v9.
- [34] C.-H. Choi, S.H. Hagvall, B.M. Wu, J.C.Y. Dunn, R.E. Beygui, C.-J.C.J. Kim, Cell interaction with three-dimensional sharp-tip nanotopography, *Biomaterials* 28 (9) (Mar. 2007) 1672–1679, doi: 10/b4qq42.
- [35] G. Jacquemet, H. Hamidi, J. Ivaska, Filopodia in cell adhesion, 3D migration and cancer cell invasion, *Curr. Opin. Cell Biol.* 36 (Oct. 2015) 23–31, doi: 10/f7xnqw.
- [36] S.D. Sackett, et al., Extracellular matrix scaffold and hydrogel derived from decellularized and delipidized human pancreas, *Sci. Rep.* 8 (1) (Dec. 2018) 10452, doi: 10/gd3dgh.
- [37] P. Newman, et al., Relationship between nanotopographical alignment and stem cell fate with live imaging and shape analysis, *Sci. Rep.* 6 (1) (Dec. 2016) 37909, doi: 10/f9dxbr.